buildings

MDPI

Article

Effect of Height-to-Diameter Ratio on the Compression Test Results of Remodeled Loess and Its Mechanism

Wang Yao [1], Xi'an Li [1,*], Youjun Wu [2], Quan Xue [3], Zhitao Hao [1], Jianfeng Shi [4], Chen Zhang [1] and Yongbiao Ren [1]

[1] College of Geological Engineering and Geomatics, Chang'an University, Xi'an 710054, China
[2] The 3rd Engineering Co., Ltd. of China Railway 16th Bureau Group, Huzhou 313000, China
[3] Institute of Rock and Soil Mechanics, Chinese Academy of Sciences, Wuhan 430071, China
[4] China Jikan Research Institute of Engineering Investigation and Design Co., Ltd., Xi'an 710043, China
* Correspondence: dclixa@chd.edu.cn

Abstract: The confined compression test is the most widely used test to study the compressive deformation of soil in a laboratory, and the height–diameter (H/D) ratio has a significant effect on the confined compression test results. However, there has been limited research on the effect of the H/D ratio on loess compression deformation. In this work, a series of confined compression tests were carried out on the remolded loess samples using a modified oedometer to explore the effect of the H/D ratio on the compression deformation. Scanning electron microscopy (SEM) tests were used to investigate the variation of the microstructure in soils with different H/D ratios along the sample height. The results showed that the axial strain of the remolded loess decreases with the increase in the H/D ratio. The influence of the H/D ratio on the compression deformation is not obvious at lower pressures and compaction degrees, but it is significantly enhanced when the H/D ratio is beyond 0.65. The compression curves of the remolded loess samples with different H/D ratios fit the Gompertz equation well, and the transition point of the compression curves becomes difficult to identify with the increase in the H/D ratio. The compression index (C_c) decreases exponentially as a function of the H/D ratio, while the compressive yield stress (P_c) increases linearly with the increase in the H/D ratio. SEM analysis showed that, with the increase in the H/D ratio, the compression deformation of the sample changed from the whole sample involved in compression to the part of the soil in contact with the pressure. The compression of loess is mainly dominated by the compression of macropores and mesopores. The development of the soil–ring wall friction on the compression deformation induced by the H/D ratio was analyzed based on the change in microstructure, and a three-stage development of the soil–ring wall friction was established. These results and analysis established the connection between the specification and the literature, providing strong support for the rationality of the confined compression test results.

Keywords: height–diameter ratio; remolded loess; confined compression test; soil–ring wall friction

check for updates

Citation: Yao, W.; Li, X.; Wu, Y.; Xue, Q.; Hao, Z.; Shi, J.; Zhang, C.; Ren, Y. Effect of Height-to-Diameter Ratio on the Compression Test Results of Remodeled Loess and Its Mechanism. *Buildings* **2023**, *13*, 176. https://doi.org/10.3390/buildings13010176

Academic Editor: Suraparb Keawsawasvong

Received: 26 November 2022
Revised: 26 December 2022
Accepted: 5 January 2023
Published: 9 January 2023

Copyright: © 2023 by the authors. Licensee MDPI, Basel, Switzerland. This article is an open access article distributed under the terms and conditions of the Creative Commons Attribution (CC BY) license (https://creativecommons.org/licenses/by/4.0/).

1. Introduction

Loess is widely distributed all over the world. In China, loess has the most extensive distribution, accounting for 6.7% of the total land area of China and 45% of Shaanxi Province [1]. In recent years, with the implementation of the Belt and Road strategy, a number of land creation projects have been carried out on the Chinese Loess Plateau [1,2]. However, geological disasters, such as land subsidence, which are closely related to loess compressibility, seriously threaten the economic development of this area [3–5]. Therefore, it is of great significance to study the compressibility of remolded loess.

The confined compression test is the classical test to study the compressibility of loess [6–8]. Although triaxial tests can accurately simulate the field stress conditions, the uniaxial tests are more widely used in engineering practices due to the advantage of being less expensive and simpler to implement. The uniaxial test has the limitation of lateral

expansion, which results in friction at the soil–ring wall contact. It has been reported that the friction will be enhanced with the increase in height–diameter (H/D) ratios [9,10], and thus affect the judgment of compressibility of test soil. Standards recommend an H/D ratio in the range of 2.5–4 to minimize the effect of friction [11,12], but its relevance has not been universally acknowledged due to the range of different soil properties. In light of this, several investigations have been conducted to ascertain how friction affects the characteristics of soil compression. Taylor [13] investigated the effect of soil–ring wall friction in consolidation tests and concluded that the thinner the sample, the less the side friction. Leonards and Girault [14] conducted consolidation tests using steel rings and found that the friction could be eliminated by applying greased Teflon when the H/D ratio exceeded six. Koolen [15] believed that the friction effect would affect the deformation characteristics of soil even at a small H/D. Kolay and Bhattacharya [16] carried out consolidation tests on kaolin soil with a large diameter (120 mm) ring coated with Teflon, and the correction factors were put forward to correct the results of conventional tests according to different consolidation characteristics. Rosine and Sabbagh [10] conducted consolidation tests on kaolin with an H/D ratio variation range of 0.5–11; the results showed that the effect of H/D ratios on the compression coefficient was the most obvious, and verified this conclusion using the finite element simulation method. Renato and Thomas [9] studied the influence of soil–ring wall friction on bulk density by combining finite element simulation and laboratory tests. The results revealed that the effect of soil–wall friction on the sample-average bulk density cannot be neglected unless $H/D < 1/8$. These previous studies and specifications proposed appropriate sample sizes for the confined tests, which ensured the rationality of the compression parameters necessary to carry out engineering activities in the area. However, there are few reports on the influence of H/D ratios on the compressive properties of loess [9,10], and the majority of the existing research concentrates on macroscopic behavior rather than its changes in the microstructure. In addition, the compression index and compressive yield stress are two key parameters to evaluate the compressive deformation of soil [17–19]. Some scholars believe that H/D has no obvious influence on compression parameters [10,20], but Kolay and Bhattacharya [16] hold the opposite opinion. The main reason for the contradiction is the interference of high moisture content and low compactness. The friction between the soil and ring wall will be reduced greatly with a higher moisture content due to lubrication [21], in which case the effect of the H/D ratio on compression parameters is almost negligible. However, the shear strength of the foundation soil will be reduced due to the high moisture content and will thus seriously threaten the safety of buildings. In addition, the effect of compactness on the relationship between the H/D ratio and compression parameters cannot be ignored [15,22,23], and a low compaction degree will also affect the safety of buildings, due to, for example, uneven settlement of foundations. Therefore, it is of practical significance to study the influence of the H/D ratio and compaction degree on the compression characteristics of loess under natural water content to ensure the long-term safety of buildings.

In this paper, the traditional consolidation instrument was modified to study the compression characteristics of remolded loess samples with different H/D ratios under different compaction degrees, and the relationship between compression parameters (compression index C_c and compressive yield stress P_c) and H/D ratios was established. SEM tests were used to quantitatively study the changes in pore distribution and microstructure in different parts of a loess sample before and after compression. The development mechanism of soil–ring wall friction was studied by combining the macroscopic compression behavior and microstructure characteristics. The findings of this study are expected to provide theoretical support for the rationality of the loess sample size used in the current confined compression test.

2. Materials and Methods

2.1. Test Materials

The loess samples were collected in Xi'an, Shaanxi Province. The loess samples were rather homogeneous in appearance and a light yellowish-brown, and the sampling depth was 5 m below ground. The basic physical property indexes of natural loess samples are shown in Table 1. According to the Unified Soil Classification System [24], the loess is classified as lean clay. The compaction curve and the particle size distribution curve are respectively presented in Figure 1a,b.

Table 1. Physical properties of the test sample.

G_s	w (%)	ρ_d (g/cm^3)	I_p	Particle Size Distribution (%)		
				Clay (<0.005 mm)	Silt (0.005~0.075 mm)	Sand (>0.075 mm)
2.71	11.91	1.43	14.12	22.86	74.36	2.78

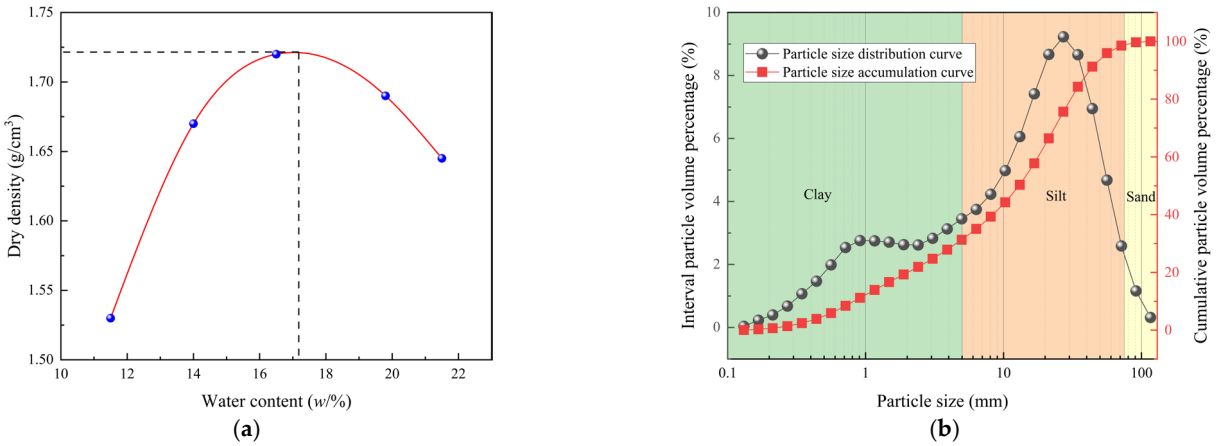


Figure 1. The compaction curve of the test loess (**a**), particle size distribution curve (**b**).

2.2. Sample Preparation

The loess samples were crushed, sieved (2 mm), and dried in an oven at 105 °C, then the loess samples were mixed with water to reach the natural moisture content (12%). Then, the mixture was placed in a moisturizing dish for more than 24 h to make the moisture fully uniform. Five H/D ratios, namely 0.32 (H = 2 cm), 0.65 (H = 4 cm), 0.97 (H = 6 cm), 1.29 (H = 8 cm), and 1.62 (H = 10 cm) were established under the same diameter (D = 6.18 cm) (Figure 2). In addition, for each H/D ratio, four different compaction degrees (K) were set: 78%, 84%, 90%, and 95%.

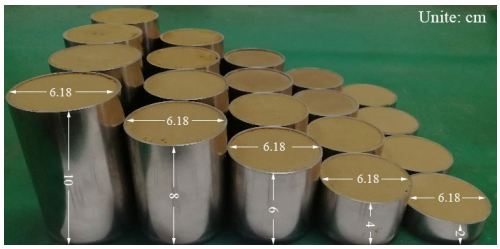


Figure 2. Remolded loess samples with different H/D ratios.

2.3. Oedometer Modification and Laboratory Compression Test

A WG-1C-type triple medium pressure oedometer was used in this test. In order to perform compression tests on samples with different H/D ratios, the oedometer needs

to be modified. Firstly, the length of the threaded segment of the original pull rod was extended by 150 mm. Secondly, the length of the original dial rod was extended by 80 mm. Thirdly, the height of the corresponding component of the sample container was increased, including the sink, a larger retaining ring, and a retaining ring. Each stacked set of components results in a 2 cm increase in the height of the sample container. The schematic diagram of the modification is shown in Figure 3. Following this was the compression test protocol for the samples with various H/D ratios. Firstly, we replaced the original pull rod and dial rod with the one that was increased in height. The component of the sample container was then superimposed to adjust the height of the sample container to match the sample height. Thirdly, we installed the specimen, and the lever was balanced in the case of close contact between the sample and the pressure transfer plate. Finally, the modified oedometer was proofread according to the geotechnical test standard (GB/T 50123-2019) [25]. The compression test could be performed after the proofreading was completed. In this test, the pressures (P) at which the samples were loaded were 50 kPa, 100 kPa, 200 kPa, 300 kPa, 400 kPa, 600 kPa, 800 kPa, and 1600 kPa, respectively. The next pressure was applied after deformation under a certain pressure was stable, and the stability standard was that the deformation under each pressure should not exceed 0.005 mm/h. The samples were removed after the compression test and allowed to air dry at room temperature before the next test.

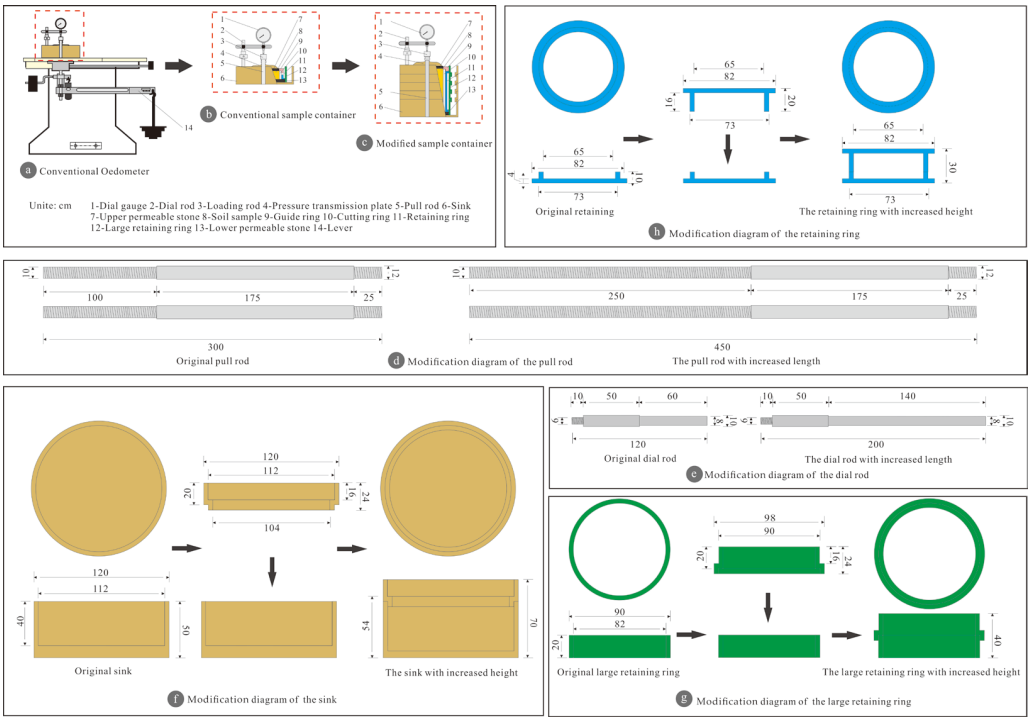


Figure 3. Schematic diagram of oedometer modification.

2.4. Calculation of the Compression Parameters

The compression data (e and P) was fitted according to the Gompertz equation by nonlinear least-squares fitting, as proposed by Gregory et al. [22]:

$$e = a + ce\{-e[b((\log_{10} P) - m)]\} \quad (1)$$

where e is the void ratio, P is the compressive stress, and a, b, c, and m are the fitting parameters.

The modulus of the slope of the virgin compression curve is commonly called the compression index C_c. There is usually an inflection point on the compression curve known as the soil precompression stress, which is regarded as a sign of compressive yield of the

soil structure [26,27]. The compressive properties of soil change at this point, and the pressure corresponding to this point is also called the compressive yield stress, P_c [27]. The C_c and P_c values are the key to further understanding the compressive properties of soil [3,28,29]. The C_c and P_c values were calculated according to the formula proposed by Gregory et al. [22]:

$$C_c = \frac{bc}{e(1)} \tag{2}$$

where b and c are the fitting parameters in Equation 1. The curvature function κ is given as follows:

$$\kappa = \frac{d^2e/d(\log_{10} P)^2}{\left\{1 + \left[de/d(\log_{10} P)\right]^2\right\}^{3/2}} \tag{3}$$

The first and second derivatives are:

$$\frac{de}{d(\log_{10} P)} = \left[bce(-e(b(\log_{10} P) - m))\right] \times \left[-e(b((\log_{10} P) - m))\right] \tag{4}$$

$$\frac{d^2e}{d(\log_{10} P)^2} = \left[b^2ce(-e(b((\log_{10} P) - m)))\right] \times \left[e(b((\log_{10} P) - m))\right] \times \left[e(b((\log_{10} P) - m)) - 1\right] \tag{5}$$

The P_c was estimated as the stress at the point of maximum curvature of the compression curve. The maximum curvature can be calculated as follows:

$$\frac{d\kappa}{d(\log_{10} P)} = 0 \tag{6}$$

2.5. Microscopic Specimen Preparation and Image Post-Processing

The preparation of the cylindrical specimens used for the SEM tests is shown in Figure 4. From each sample, five cylindrical specimens were cut, with the exception of the cylinders that were cut from the top and bottom, with an H/D ratio of 0.32 prior to compression. All cylindrical specimens were cut from remolded samples with compaction degrees from 78% to 95%. All cylindrical specimens were numbered (Figure 5a), where b and a represented before and after compression, respectively; the number after the letter represented the height of the remolded sample, and the number after the horizontal line represented the position of the cylindrical specimen in the remolded specimen. For example, a10-1 denoted the cylindrical specimen was cut from the first layer of the remolded sample with a height of 10 cm (H/D ratio 1.62) after compression. After the treatment of glue injection, polishing, and gold spraying, the cylindrical specimens were observed, and images were collected by the Quanta FEG scanning electron microscope system. In this study, image processing software (IPP) was used to process the collected SEM images and data acquisition. More details of the SEM tests and IPP image processing can be found in the literature by Li et al. and Wang et al. [1,30].

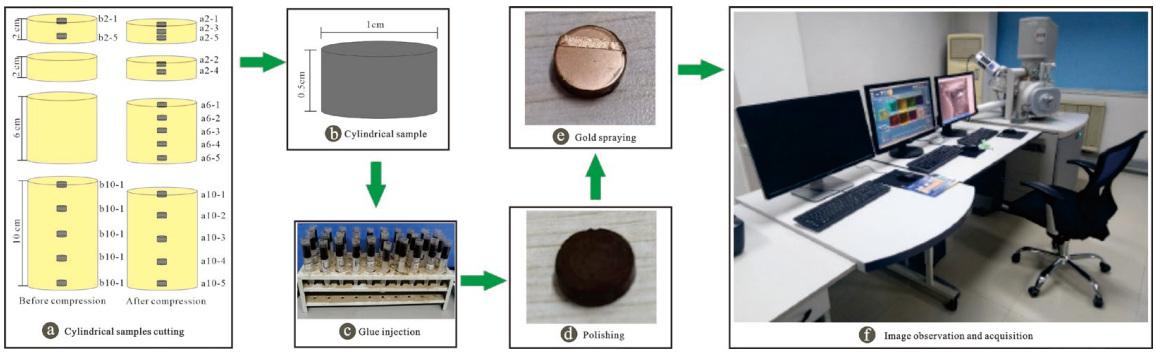


Figure 4. Preparation of cylindrical specimens for SEM tests.

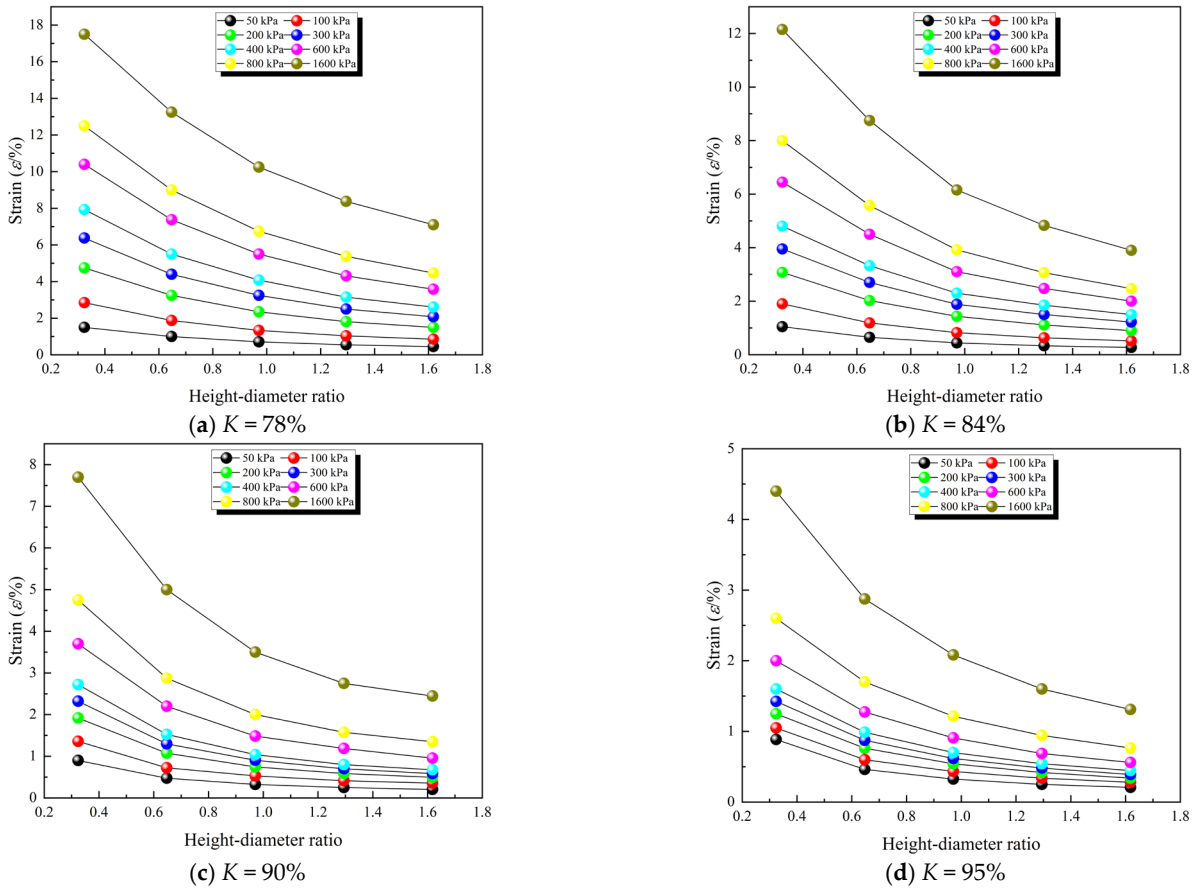


Figure 5. The relationship between strain and H/D ratios under different compaction degrees.

3. Results and Discussion

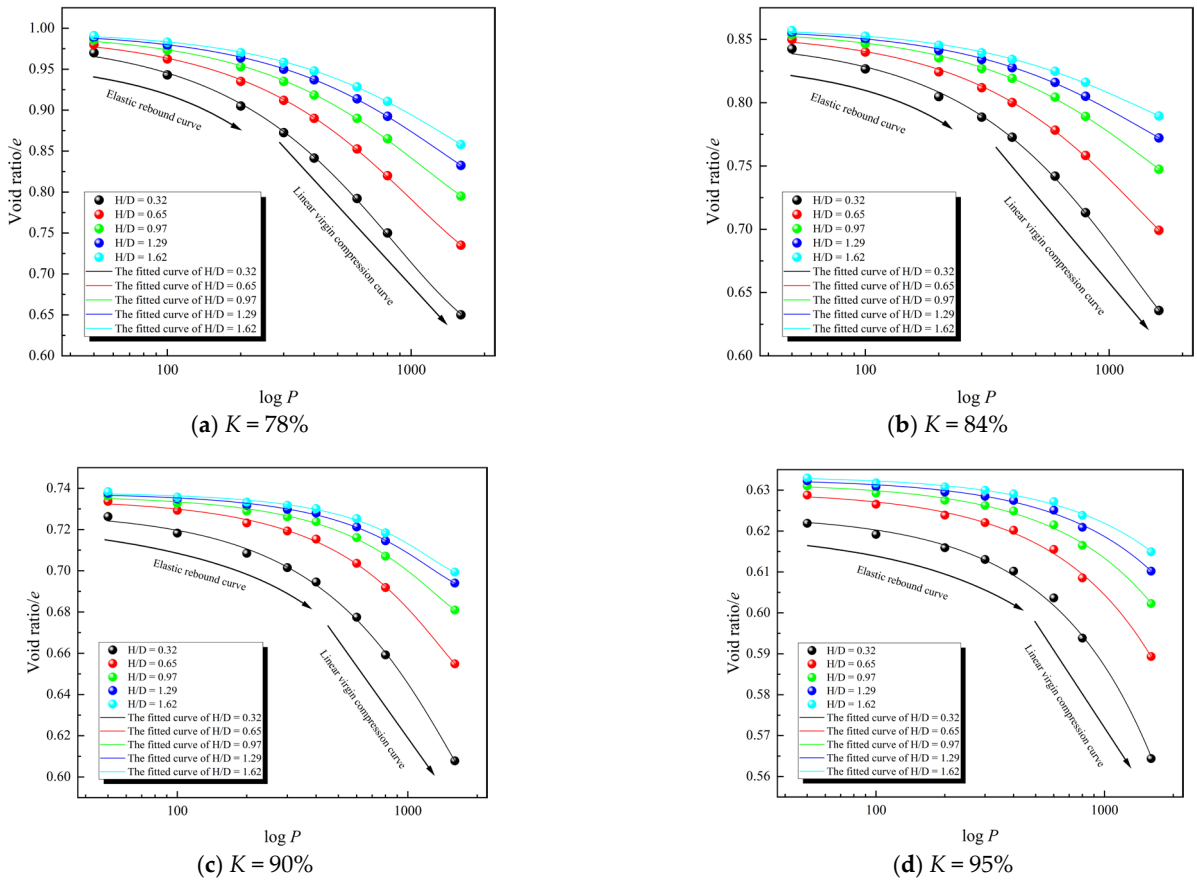
3.1. The Relationship between Axial Strain and H/D Ratios

Figure 5 shows the variation of axial strain with H/D ratios under different compaction degrees. We found that the axial strain decreases with the increase in H/D ratios and compaction degree. At the compaction degree of 78%, the axial strains with an H/D ratio of 0.32 and 1.62 at 50 kPa and 1600 kPa were 1.51%, 0.48% and 17.51%, and 7.11%, respectively. The results indicated that the larger the H/D ratio at the same pressure, the more difficult the sample was to compress. This is because as the H/D ratio increases, the friction area between the soil and the ring wall increases, and the soil–ring wall friction exerts an upward resistance on the sample, weakening the compaction effect of the external force on the sample. As the compaction degree increased to 95%, the axial strains at 50 kPa and 1600 kPa decreased to 0.89%, 0.21% and 4.41%, and 1.31% for samples with an H/D ratio of 0.32 and 1.62, respectively. The results indicated that the higher the compaction degree, the more difficult the sample is to compress. This is because the increase in compaction degree increases the content of soil particles per unit area of the ring wall [10,16], which also weakens the compression effect of the external force on the sample. Comparing the axial strains at different compaction degrees and different pressures, we found that the axial strains with varied H/D ratios have the lowest differences at lower pressures and compaction degrees. This result indicates that the effect of the H/D ratio on the compression deformation of remodeled loess is not significant at smaller pressures and compaction degrees. This can be attributed to the friction between soil particles and the ring wall not being as intense at lower pressures and compaction degrees. In addition, it was discovered that, when the compaction degree surpasses 84%, the variation of the axial strain first decreases quickly and then gradually as the H/D ratios rise, and the variation tendency becomes more pronounced as pressure rises. At this time, we found that there was an

obvious transition in the axial strain at the H/D ratio of 0.65. The results revealed that the attenuating effect of the H/D ratio on the compression deformation of the remodeled loess sample was significantly enhanced once the H/D ratio is >0.65, especially when the compaction degree is >84%. This result also proved that the sample size (H/D = 0.32) currently being utilized is within a reasonable range (H/D < 0.65) and provided strong support for the rationality of the compression test results of remolded loess.

3.2. The Compression Curves

Figure 6 displays the compression curves for various H/D ratios under different compaction degrees. The fitting results are shown as solid lines in the figures. As expected, the compression curves with the higher H/D ratios were always on top of those with the lower ones. It was discovered that the Gompertz equation could accurately describe the compression curve (all R^2 values are over 0.9), indicating that the development of compressive deformation of remolded loess is not affected by the H/D ratio. The identification of the transition between the elastic rebound curve and the virgin compression curve at the same compaction degree became more challenging as the H/D ratio rose. This can be attributed to the friction applied on the samples increasing with the increase in the H/D ratio. The strain of the sample decreases at the same pressure, and the compression curve is flatter, so the transition point was not easily identified. In contrast, the identification of transition becomes easier with an increase in the compaction degree for the same H/D ratio. This can be interpreted as the soil structure becoming more compact with the increase in compaction degree from 78% to 95%. The slope of the elastic rebound curve with an H/D ratio of 0.32 was reduced by 68.97%, while it was reduced by 63.48% for an H/D ratio of 1.62. The elastic rebound curve became flatter due to fewer pores to compress. As a result, the transition point was simpler to locate.



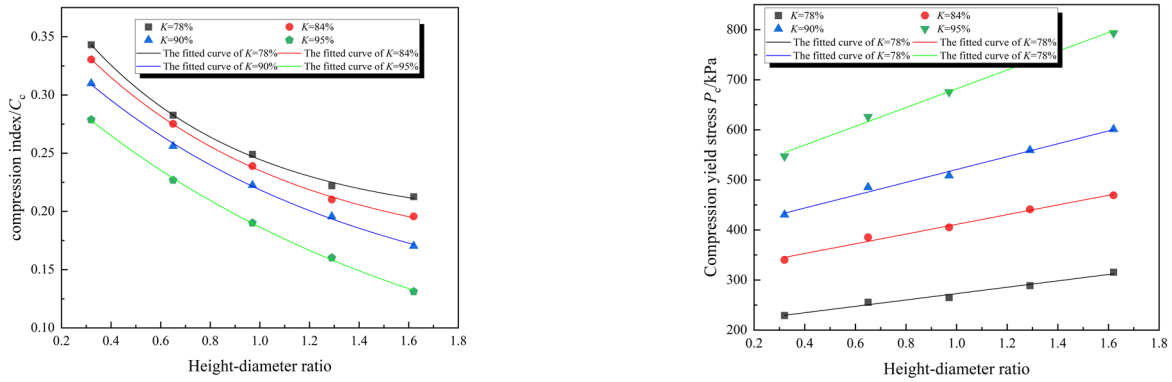
(**a**) K = 78% (**b**) K = 84%

(**c**) K = 90% (**d**) K = 95%

Figure 6. The compression curves of different H/D ratios under various compaction degrees.

3.3. Compression Parameters

Figure 7 shows the variation of compression parameters with the H/D ratio. It was found that the compression index (C_c) decreases with the increase in the H/D ratio and compaction degree. As the H/D ratio increased from 0.32 to 1.62, the decrease of C_c rose from 38.01% of the compaction degree of 78% to 56.77% of the compaction degree of 95%. As the compaction degree increased from 78% to 95%, the decrease of C_c rose from 24.51% for an H/D ratio of 0.32 to 47.38% for an H/D ratio of 1.62. This result indicated that the effect of the H/D ratio on the C_c of remolded loess is greater than that of the compaction degree. With an increase in compaction degree, the difference between neighboring *Cc* with the same H/D ratio grows. This can be attributed to the capacity of pores to withstand compression at the same pressure, which increases with the increase in compaction degree. At the same compaction degree, the slope between adjacent C_c values decreased with an increasing H/D ratio, and a significant decrease was observed at the H/D ratio of 0.65 for the compaction degree of 78%. The slope tends to decrease steadily when the H/D ratio exceeds 0.65 with the increase in compaction degree. This suggests that the weakening effect of soil–ring wall friction on compression deformation of remodeled loess was enhanced significantly when the H/D ratio exceeded 0.65, and it developed stably with the increase in compaction degree. In addition, the compressibility of the sample will be underestimated with the increase in the H/D ratio. As a result, the compression deformation of the foundation may exceed the design value, endangering the safety of the building. As for compressive yield stress (P_c), it was found to increase with the increase in the H/D ratio and compaction degree. As the H/D ratio increased from 0.32 to 1.62, the increment of P_c increased from 37.66% with a compaction degree of 78% to 44.94% with a compaction degree of 95%. However, as the compaction degree rose from 78% to 95%, the increase in P_c rose from 138.65% of 0.32 to 152.68% of 1.62. This result suggested that the effect of the compaction degree on P_c is greater than the H/D ratio, and the increase in the H/D ratio and compaction degree improved the maximum pressure that the soil can withstand before plastic deformation. In addition, we fitted the compression parameters, and the fitting results are shown in Table 2. The relationship between C_c and the H/D ratio fulfills an exponential function, while there is a positive linear correlation between P_c and the H/D ratio.



(**a**) Compression index (**b**) Compression yield stress

Figure 7. The relationship between compression parameters and H/D ratios.

Table 2. Fitting results of compression parameters.

Compactness (K/%)	Compression Index (C_c)		Compressive Yield Stress (P_c)	
	Fitting Formula	R^2	Fitting Formula	R^2
78	$C_c = 0.19 + 0.25e^{(-1.51\ H/D)}$	0.99	$P_c = 209.29 + 63.58H/D$	0.98
84	$C_c = 0.16 + 0.25e^{(-1.17\ H/D)}$	0.99	$P_c = 314.13 + 96.99H/D$	0.99
90	$C_c = 0.11 + 0.27e^{(-0.86\ H/D)}$	0.99	$P_c = 392.39 + 128.42H/D$	0.99
95	$C_c = 0.03 + 0.31e^{(-0.66\ H/D)}$	0.99	$P_c = 494.85 + 187.12H/D$	0.99

3.4. Variation of the Pore Area Ratio and Distribution of Pores along the Sample Height

The ratio of the pore area of the two-dimensional microscopic image obtained by SEM tests to the total area of the image, which is called the pore area ratio (PAR), is typically employed to quantitatively analyze the variation of the soil microstructure due to its high correspondence with deformation [1,31]. PAR and stress have an inverse relationship; the latter results in a reduced external force on the soil when the former is greater. The PAR values of different layers along the sample height with H/D ratios of 0.32, 0.97, and 1.62 after compression are presented in Figure 8. For the sample with an H/D ratio of 0.32, the PAR of different compaction degrees was found to vary insignificantly along the sample height, and the PAR values of different stratifications with different compaction degrees were all compressed to about 13%. Contrarily, for samples with an H/D ratio of 0.97 and 1.62, the PAR was found to increase rapidly at first and then slowly along the sample height. The obvious compression of PAR for different compaction degrees was predominantly concentrated in the range from the top to the middle layer of the samples, with little change in the bottom layer. Particularly at the compaction degree of 95%, the PAR remained almost consistent from the second layer. This outcome is comparable to that found by earlier studies [10,16]. This difference trend suggested that, as the H/D ratio increases, the compressive deformation of the remodeled loess shifts from being caused by the entire sample to being primarily caused by the portion of the soil that is in contact with the pressure, and the hindrance effect of the compaction degree on the compressive deformation of remolded loess is less noticeable when the H/D ratio is small. Therefore, a sample with a smaller H/D ratio should be selected for compression tests under confined conditions. Additionally, the H/D ratio of 0.32 had the least impact on compression when compared to other H/D ratios. This conclusion provides strong support again for the rationality of the experimental results obtained by the size of the sample utilized in the current compression test.

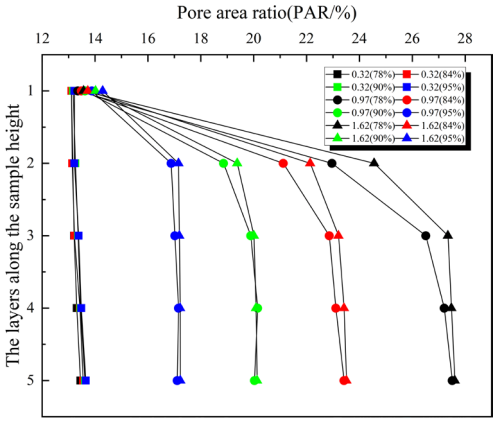
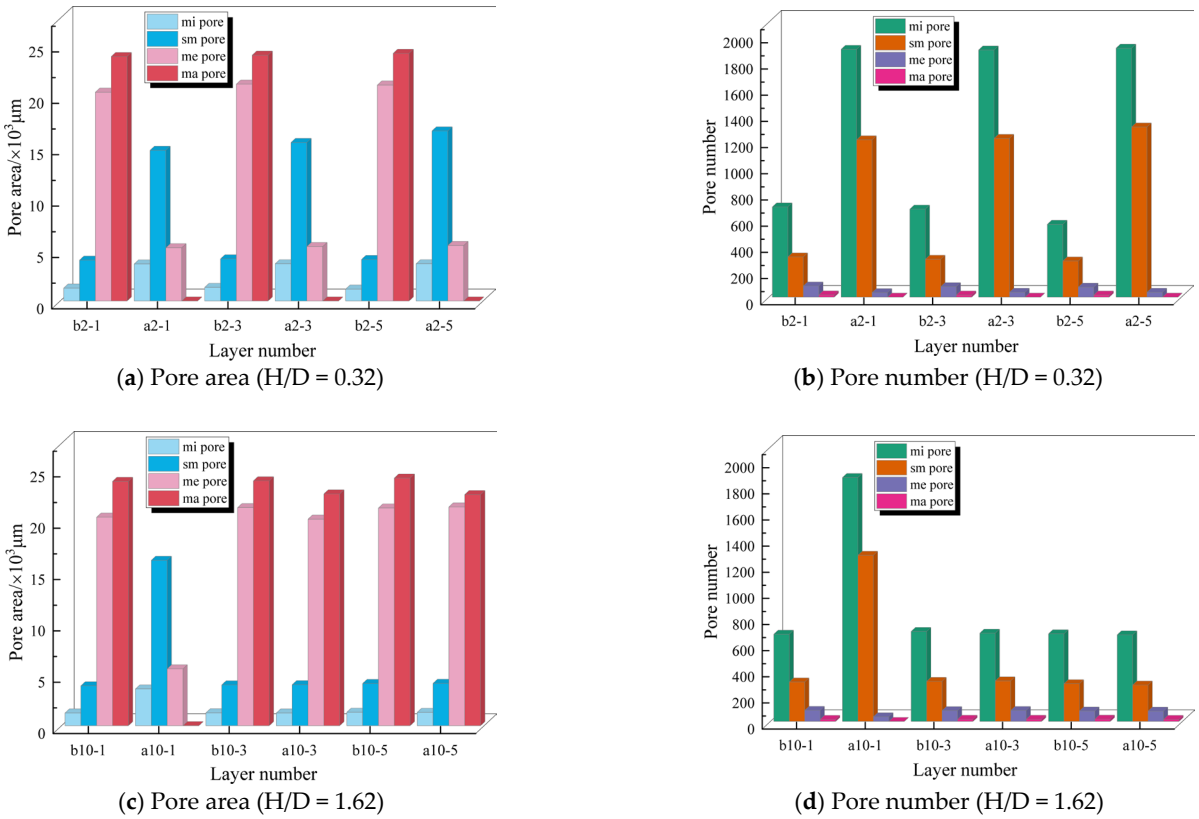


Figure 8. Variation of PAR with different H/D ratios along the sample height after compression.

The distribution of pores is a direct reflection of variation in soil structure. The pores in loess can be classified into four types based on their mean radius [32]: micropores (<1 μm), small pores (1–4 μm), mesopores (4–32 μm), and macropores (>32 μm). Figure 9

illustrates the distribution of pores in different layers with the H/D ratio of 0.32 and 1.62 at a compaction degree of 78%. The distribution of the same type of pores varied little across all layers before compression, with the largest differences in the area of macropores, mesopores, small pores, and micropores of 1.38%, 4.36%, 5.42%, and 11.81%, respectively, and the largest differences in pore numbers of 11.11%, 10.61%, 10.11%, and 19.31%, respectively. This suggests that the remolded loess sample was uniform, and the influence of sample inhomogeneity on test results can be ignored. After compression, the changes in pores at different H/D ratios showed obvious differences. For an H/D ratio of 0.32, the area of macropores and mesopores in different layers decreased by approximately 96% and 74%, while the decrease was approximately 95% and 55% for their number. Meanwhile, the area of micropores and small pores in different layers increased by about 200% and 300%, while the increase was about 200% and 330% for their number. At an H/D ratio of 1.62, the first layer showed the most noticeable pore alteration, which was the same as the H/D ratio of 0.32. The area and number of pores in the fifth layer were almost unchanged from before compression. The results showed that, as the H/D ratio increased, the compression of remolded loess was mainly dominated by macropores and mesopores, while small pores and micropores contributed little to the compression. This can be ascribed to the significant instability of the structure of the macropores and mesopores, which makes them more vulnerable to pressure destruction [33,34].



(**a**) Pore area (H/D = 0.32)

(**b**) Pore number (H/D = 0.32)

(**c**) Pore area (H/D = 1.62)

(**d**) Pore number (H/D = 1.62)

Figure 9. The distribution of pore area and pore number at the compaction degree of 78%.

3.5. Mechanism Analysis of Development of Soil–Ring Wall Friction Based on the Microstructure

SEM images of the first and fifth layers with an H/D of 0.32 and 1.62 before and after compression at the compaction degree of 78% are shown in Figure 10. Before compression, the soil was relatively loose and the coarse particles (mainly silt) mostly existed in the form of individual particles, while the clay particles and cementing materials existed as aggregates. Direct contact (including direct point-to-point contact and direct face-to-face contact) between particles was dominant. The surface of coarse particles is relatively clean

and, therefore, they can easily slide and rotate. Pore area as a percentage was relatively high, and a connection was clearly present. This structure makes the soil more susceptible to external force; therefore, obvious void ratio changes can be observed in the early stage of compression tests [1,33]. After compression, except for a10-5, the soil structure became more compact, the macropores were obviously compressed, and the proportion of the pore area decreased significantly. The coarse particles were closely wrapped by clay and cementing material and connected to other coarse particles in the form of indirect cementing connections. As a result, there was greater interlocking between the particles, making it more difficult for the coarse particles to rotate or slide. Even under high pressure, the soil was more stable due to this structure [1,33]. However, the soil structure of a10-5 was the same as that before compression and did not seem to be compressed, indicating that the compression of the soil structure mainly occurred in the top layer with the increase of the H/D ratio.

The clay and cementing materials in loess often reside as aggregate in the soil pores after remolding [35]. In the initial stage of compression (Figure 11-1), the loess sample is essentially in a state of overall compression. The deformation of the soil sample was mainly manifested by the compression of macropores and mesopores (Figure 11b), and the number of soil particles per unit area increased as the soil–ring wall friction began to increase. Small pores and micropores developed at this stage (Figure 11c). At this time, for a small H/D ratio, the distribution of stress in the sample was almost unchanged along the sample height due to the small friction area (Figure 11a), and the sample tended to be compressed as a whole. For a large H/D ratio, the stress of the soil sample decreased gradually along the sample height as a result of the increased friction area (Figure 11A), and the compression of the sample began to display partial compression. At this stage, although there was a noticeable reduction in pore space, the interaction between the soil particles and the ring wall was not yet very intense. The deformation of the soil was considered recoverable at this stage once the external force was removed [22]. Therefore, this stage corresponded to the elastic rebound curve stage. As the pressure increased, the pores were further compressed, the coarse particles began to adjust their spatial position to form a more compact state, and the aggregates of clay particles and cementing materials were compressed and migrated through the pores [36], filling the pores and coating the surface of coarse particles to form a coating structure [1,30] (Figure 11-2). The connection form of coarse particles changed from the original direct connection to an indirect cemented connection, resulting in an obvious increase in soil–ring wall friction (Figure 11d). At this time, for a small H/D ratio, the stress distribution began to decrease along the sample height. For a large H/D ratio, the distribution of stress along the sample height showed a rapid decrease at first and then a gradual decrease. The interaction between the soil particles and the ring wall was the most apparent, which means that the increased rate of soil–ring wall friction is the largest. In this stage, the original structure was entirely destroyed and a new structure was formed. Therefore, this stage corresponds to the compression yield stage. As the pressure continued to increase, the soil particles underwent slip while crushing at the direct connection and the contact with the ring wall (Figure 11-3). Renato and Thomas [9] found that significant friction occurred at the contact between the soil and the ring wall by simulating the stress distribution in soil under confined compression. In this process, the rough surface of coarse particles due to crushing increased the friction coefficient μ, and the debris generated by particle crushing filled the pore space, increasing the number of soil particles per unit area (Figure 11e). As a result, the friction force further increased. However, due to the limited particle crushing and slippage, the increased rate of friction with pressure in this stage was smaller than that in the previous stage. For different H/D ratios, the stress distribution was identical to that of the preceding stage, but to a greater extent. In this stage, the interaction between the soil particles and the ring wall increased steadily with the increase in pressure. Therefore, the soil–ring wall friction in this stage developed steadily with the increase in pressure, but at a slower pace than in the stage before. Therefore, this stage corresponds to the linear virgin compression curve stage.

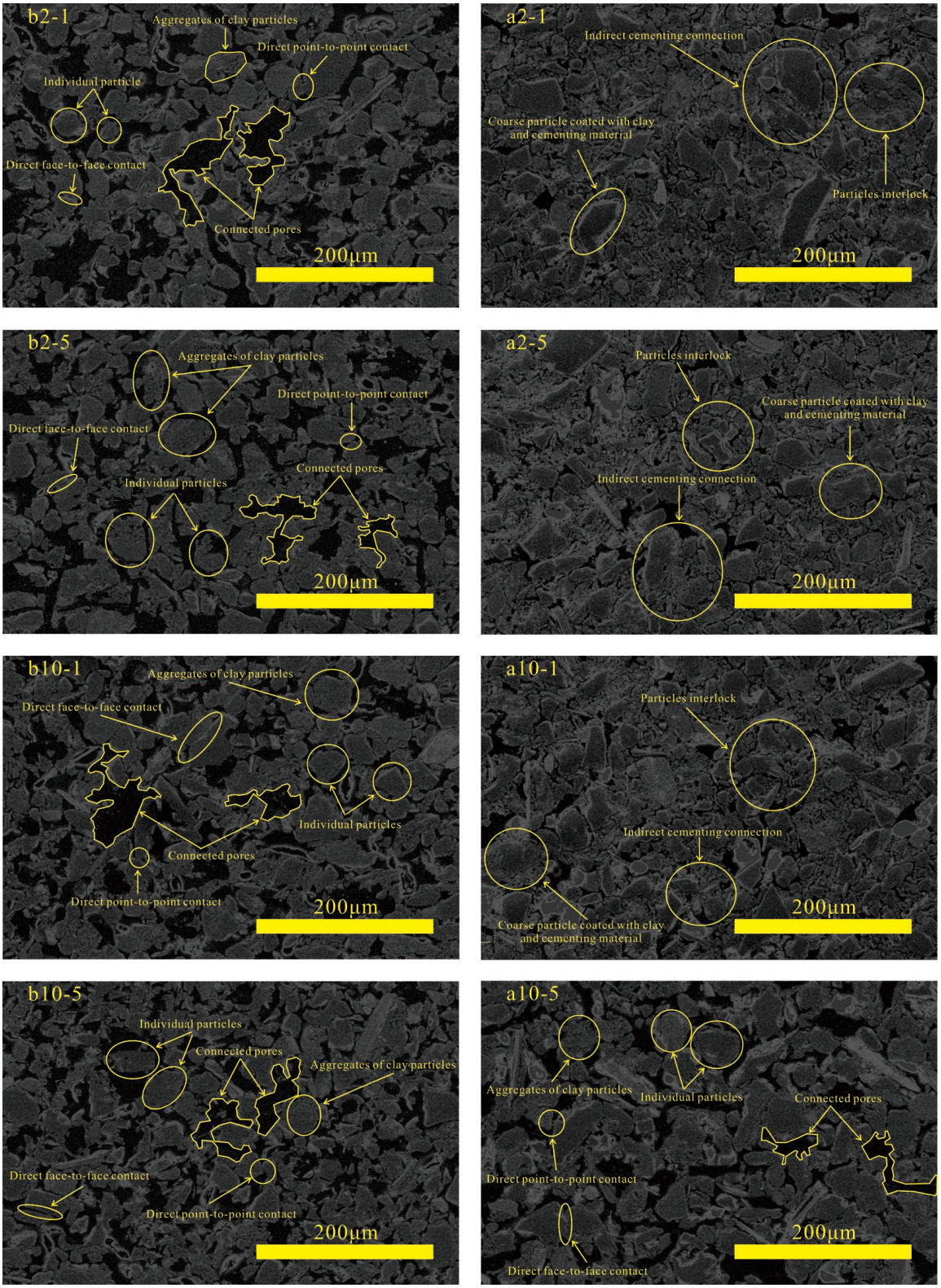


Figure 10. SEM images of remolded loess samples: letter b and a represent before and after compression, respectively; numbers after the letter represent the sample height; numbers after the horizontal line represent the position of the cylindrical specimen in the remolded sample.

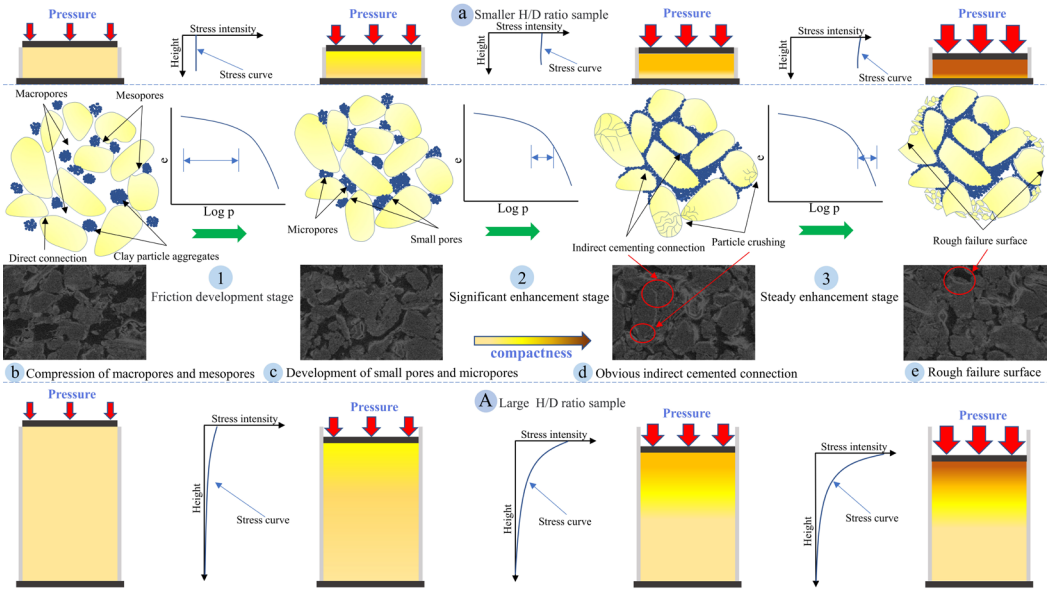


Figure 11. Schematic diagram of the development of soil–ring wall friction during compression.

4. Conclusions

(1) The greater the H/D ratio, the more difficult it is to compress a specimen. The effect of the H/D ratio on the compressive deformation of remolded loess is not evident at a lower compaction degree and pressure, but it is greatly amplified when the H/D ratio exceeds 0.65. The dimensions of the ring currently used in the confined compression test are within a reasonable range.

(2) The development of compressive deformation of remolded loess is unaffected by the H/D ratio, and the compression curves of different H/D ratios satisfy the Gompertz equation. With an increase in the H/D ratio, the transition between the elastic rebound curve and the virgin compression curve becomes more difficult to recognize.

(3) The effect of the H/D ratio on the *Cc* of remolded loess is greater than that of the compaction degree, but the effect on *Pc* is the opposite. The C_c decreases exponentially with an increasing H/D ratio, while the *Pc* increases linearly.

(4) With an increase in the H/D ratio, the compression of the remodeled loess sample shifts from the involvement of the whole sample to that of the soil in contact with the pressure. Macropores and mesopores mostly contribute to the compression of loess samples.

(5) The development of soil–ring wall friction in remodeled loess during compression occurred in three stages: development, significant enhancement, and stable enhancement. The movement of clay particles and the crushing of coarse particles are the most influential variables in the formation of soil–ring wall friction.

Author Contributions: Conceptualization, W.Y. and X.L.; methodology, W.Y., X.L., Y.W., Q.X., Z.H. and J.S.; software, W.Y., Y.W., Q.X., Z.H., J.S. and C.Z.; validation, X.L., W.Y., Y.W., J.S., C.Z., and Y.R.; formal analysis, W.Y., Y.W., Z.H., J.S. and C.Z.; investigation, W.Y., Y.W., Q.X., J.S. and C.Z.; resources, X.L., Y.W., Y.R.; data curation, W.Y., Q.X., J.S. and C.Z.; writing—original draft preparation, W.Y., Q.X., Z.H. and Y.R.; writing—review and editing, W.Y.; visualization, Y.W., Q.X., Z.H., C.Z. and Y.R.; supervision, X.L., Z.H. and Y.R.; project administration, X.L. and Y.R.; funding acquisition, X.L. All authors have read and agreed to the published version of the manuscript.

Funding: This research was funded by the National Natural Science Foundation of China, grant numbers 42230712 and 41877225.

Institutional Review Board Statement: Not applicable.

Informed Consent Statement: Not applicable.

Data Availability Statement: Not applicable.

Conflicts of Interest: The authors declare no conflict of interest.

References

1. Li, X.-A.; Li, L.; Song, Y.; Hong, B.; Wang, L.; Sun, J. Characterization of the mechanisms underlying loess collapsibility for land-creation project in Shaanxi Province, China—A study from a micro perspective. *Eng. Geol.* **2019**, *249*, 77–88. [CrossRef]
2. Wu, J.H.; Li, P.Y.; Qian, H.; Destech Publicat, I. Opportunities and Challenges Associated with the World's Largest Geotechnical Engineering Project for Land Creation on the Loess Plateau. In Proceedings of the International Conference on Computer Science and Environmental Engineering (CSEE 2015), Beijing, China, 17–18 May 2015; pp. 141–147.
3. Zuo, L.; Lyu, B.; Xu, L.; Li, L. The influence of salt contents on the compressibility of remolded loess soils. *Bull. Eng. Geol. Environ.* **2022**, *81*, 185. [CrossRef]
4. Li, Z.; Qi, Z.; Qi, S.; Zhang, L.; Hou, X. Microstructural changes and micro-macro-relationships of an intact, compacted and remolded loess for land-creation project from the Loess Plateau. *Environ. Earth Sci.* **2021**, *80*, 593. [CrossRef]
5. Chen, G.; Zhang, Y.; Zeng, R.; Yang, Z.; Chen, X.; Zhao, F.; Meng, X. Detection of Land Subsidence Associated with Land Creation and Rapid Urbanization in the Chinese Loess Plateau Using Time Series InSAR: A Case Study of Lanzhou New District. *Remote Sens.* **2018**, *10*, 270. [CrossRef]
6. Wang, L.; Shao, S.; She, F. A new method for evaluating loess collapsibility and its application. *Eng. Eng. Geol.* **2020**, *264*, 105376. [CrossRef]
7. Jia-Wei, L.; Heng-Hui, F.; Xin-Ye, S.; Xiu-Juan, Y. Characteristics of Shear Strength and Deformation of Compacted Q3 Loess. *Soil Mech. Found. Eng.* **2020**, *57*, 65–72. [CrossRef]
8. Zhuangfu, Z.; Yanpeng, Z.; Shuaihua, Y. Study on settlement deformation of high fill foundation in large thickness loess area. *Arab. J. Geosci.* **2021**, *14*, 1173. [CrossRef]
9. de Lima, R.P.; Keller, T. Impact of sample dimensions, soil-cylinder wall friction and elastic properties of soil on stress field and bulk density in uniaxial compression tests. *Soil Tillage Res.* **2019**, *189*, 15–24. [CrossRef]
10. Rosine, L.T.N.; Toma, S.T.M. The impact of the diameter to height ratio on the compressibility parameters of saturated fine-grained soils. *IJERT* **2015**, *04*, 8–19.
11. *D2435*; Standard Test Method for One Dimensional Consolidation Properties of Soils. American Society for Testing and Material: West Conshohocken, PA, USA, 2010.
12. *BS1377*; Methods of Tests for Soils for Civil Engineering Purposes—Compressibility, Permeability and Durability Tests. British Standard: London, UK, 1990.
13. Taylor, D.W. *Research on Consolidation of Clays*; Massachusetts Institute of Technology: Cambridge, UK, 1942.
14. Leonards, G.A.; Girault, P. A study of the one-dimensional consolidation test. In Proceedings of the Fifth International Conference on Soil Mechanics and Foundation Engineering, Paris, France, 17–22 July 1961; pp. 213–218.
15. Koolen, A.J. A method for soil compactibility determination. *J. Agric. Eng. Res.* **1974**, *19*, 271–278. [CrossRef]
16. Kolay, P.; Bhattacharya, G. Remediation of the side friction in conventional oedometer tests by using large diameter consolidometer ring. *Int. J. Geotech. Eng.* **2008**, *2*, 161–167. [CrossRef]
17. Tiwari, B.; Ajmera, B. Consolidation and swelling behavior of major clay minerals and their mixtures. *Appl. Clay Sci.* **2011**, *54*, 264–273. [CrossRef]
18. Habibbeygi, F.; Nikraz, H.; Verheyde, F. Determination of the compression index of reconstituted clays using intrinsic concept and normalized void ratio. *Int. J. Geomate* **2017**, *13*, 54–60. [CrossRef]
19. Mun, W.; Coccia, C.J.R.; McCartney, J.S. Application of Hysteretic Trends in the Preconsolidation Stress of Unsaturated Soils. *Geotech. Geol. Eng.* **2018**, *36*, 193–207. [CrossRef]
20. Lei, H.Y.; He, C.F.; Qiu, W.W.; Chen, L. Experimental Study on the Effect of Size Effect on Consolidation Characteristics of Soft Soil Filled by Blowing. *J. Tianjin Univ. Nat. Sci. Eng. Technol. Ed.* **2016**, *49*, 73–79.
21. Jiang, Y.; Yi, Y.; Tian, T.; Sha, H.; Fan, J.; Ji, X.; Xue, J. Water Infiltration and Water Stability of Compacted Loess Roadbeds Based on Vibration Compaction. *Arab. J. Sci. Eng.* **2022**, *47*, 4987–5001. [CrossRef]
22. Gregory, A.S.; Whalley, W.R.; Watts, C.W.; Bird, N.R.A.; Hallett, P.D.; Whitmore, A.P. Calculation of the compression index and precompression stress from soil compression test data. *Soil Tillage Res.* **2006**, *89*, 45–57. [CrossRef]
23. Cetin, H. Soil-particle and pore orientations during consolidation of cohesive soils. *Eng. Geol.* **2004**, *73*, 1–11. [CrossRef]
24. *ASTM Standard D2487*; Standard Practice for Classification of Soils for Engineering Purposes (Unified Soil Classification System). ASTM International: West Conshohocken, PA, USA, 2011.
25. *GB/T 50123-2019*; Geotechnical Test Standard. National Standard of China: Beijing, China, 2019.
26. Jiang, M.; Zhang, F.; Hu, H.; Cui, Y.; Peng, J. Structural characterization of natural loess and remolded loess under triaxial tests. *Eng. Geol.* **2014**, *181*, 249–260. [CrossRef]
27. Meng, J.; Li, X.-A. Effects of carbonate on the structure and properties of loess and the corresponding mechanism: An experimental study of the Malan loess, Xi'an area, China. *Bull. Eng. Geol. Environ.* **2019**, *78*, 4965–4976. [CrossRef]
28. Jian, T.; Kong, L.; Bai, W.; Sun, Z. Investigation on compressibility and microstructure evolution of intact loess at different wetting state. *Front. Earth Sci.* **2022**, *10*, 923358. [CrossRef]

29. Shao, S.; Wang, Z.; Shao, S. Evaluation Method for Self-Weight Collapse Deformation of Tunnel Foundations in Thick Loess. *Soil Mech. Found. Eng.* **2022**, *59*, 57–67. [CrossRef]
30. Wang, L.; Li, X.-A.; Li, L.-C.; Hong, B.; Yao, W.; Lei, H.-n.; Zhang, C. Characterization of the collapsible mechanisms of Malan loess on the Chinese Loess Plateau and their effects on eroded loess landforms. *Hum. Ecol. Risk Assess.* **2020**, *26*, 2541–2566. [CrossRef]
31. Li, L.; Li, X.-A.; Wang, L.; Hong, B.; Shi, J.; Sun, J. Correction to: The effects of soil shrinkage during centrifuge tests on SWCC and soil microstructure measurements. *Bull. Eng. Geol. Environ.* **2021**, *80*, 731–733. [CrossRef]
32. Lei, X.Y. Pore types of loess soils in China and its collapsibility. *Sci. China B* **1987**, *12*, 1310–1316.
33. Luo, H.; Wu, F.; Chang, J.; Xu, J. Microstructural constraints on geotechnical properties of Malan Loess: A case study from Zhaojiaan landslide in Shaanxi province, China. *Eng. Geol.* **2018**, *236*, 60–69. [CrossRef]
34. Wang, J.-D.; Li, P.; Ma, Y.; Vanapalli, S.K. Evolution of pore-size distribution of intact loess and remolded loess due to consolidation. *J. Soils Sediments* **2019**, *19*, 1226–1238. [CrossRef]
35. Mu, Q.Y.; Zhou, C.; Ng, C.W.W. Compression and wetting induced volumetric behavior of loess: Macro- and micro-investigations. *Transp. Geotech.* **2020**, *23*, 100345. [CrossRef]
36. Wei, Y.-n.; Fan, W.; Yu, B.; Deng, L.-s.; Wei, T. Characterization and evolution of three-dimensional microstructure of Malan loess. *Catena* **2020**, *192*, 104585. [CrossRef]

Disclaimer/Publisher's Note: The statements, opinions and data contained in all publications are solely those of the individual author(s) and contributor(s) and not of MDPI and/or the editor(s). MDPI and/or the editor(s) disclaim responsibility for any injury to people or property resulting from any ideas, methods, instructions or products referred to in the content.